Realizing Fractional Chern Insulators in Dipolar Spin Systems

N. Y. Yao, A. V. Gorshkov, C. R. Laumann, A. M. Läuchli, J. Ye, and M. D. Lukin

Realizing Fractional Chern Insulators in Dipolar Spin Systems

N. Y. Yao[1*], A. V. Gorshkov[2], C. R. Laumann[1,3], A. M. Läuchli[4], J. Ye[5], M. D. Lukin[1]

[1]*Physics Department, Harvard University, Cambridge, MA 02138, U.S.A.*
[2]*Institute for Quantum Information and Matter,*
California Institute of Technology, Pasadena, CA 91125, U.S.A.
[3]*ITAMP, Harvard-Smithsonian Center for Astrophysics, Cambridge, MA 02138, U.S.A.*
[4]*Institute for Theoretical Physics, University of Innsbruck, A-6020 Innsbruck, Austria*
[5]*JILA, National Institute of Standards and Technology and University of Colorado,*
Department of Physics, University of Colorado, Boulder, Colorado 80309, USA and
[*]*e-mail: nyao@fas.harvard.edu*

Strongly correlated quantum systems can exhibit exotic behavior controlled by topology. We predict that the $\nu = 1/2$ fractional Chern insulator arises naturally in a two-dimensional array of driven, dipolar-interacting spins. As a specific implementation, we analyze how to prepare and detect synthetic gauge potentials for the rotational excitations of ultra-cold polar molecules trapped in a deep optical lattice. With the motion of the molecules pinned, under certain conditions, these rotational excitations (acting as effective spins) form a fractional Chern insulating state. We present a detailed experimental blueprint for its realization and demonstrate that the implementation is consistent with near-term capabilities. Prospects for the realization of such phases in solid-state dipolar systems are discussed as are their possible applications.

The quest to realize novel forms of topological quantum matter has recently been galvanized by the notion of fractional Chern insulators - exotic phases, which arise when strongly interacting particles inhabit a flat topological bandstructure [1–8]. Particles injected into these exotic states of matter fractionalize into multiple independently propagating pieces, each of which carries a fraction of the original particle's quantum numbers. While similar effects underpin the fractional quantum Hall effect observed in continuum two dimensional electron gases [10, 11], fractional Chern insulators, by contrast, are lattice dominated. They have an extremely high density of correlated particles whose collective excitations can transform non-trivially under lattice symmetries [8, 9, 12].

In this Letter, we predict the existence of a fractional Chern insulator in dipolar interacting spin systems. This state exhibits fractionalization of the underlying spins into quasiparticle pairs with semionic statistics [13, 14]. The predicted FCI state may also be viewed as a gapped chiral spin liquid (CSL) [13, 15].

Several recent studies have conjectured the existence of fractionalized topological phases in idealized lattice models that require sensitively tuned long-range hopping and interactions [5–7, 16–18]. Broadly speaking, two single-particle microscopic ingredients are required. First, the dispersion of the lattice band-structure must be quenched relative to the energy scale of interactions [16–18]. Second, the flat band should possess a non-trivial Chern number, reflecting the underlying Berry phase accumulated by a particle moving in the band-structure. To observe a *fractionalized* insulating state, one must partially fill the topological flat band-structure with interacting particles; since the FCI state generally competes with superfluid and crystalline orders, the resulting phase diagram naturally exhibits both conventional and topological phases (Fig. 1). Up to now, it has been unclear whether such exotic fractional Chern insulating phases can be realized in any real-world physical system.

We consider a two-dimensional array of tilted, driven, generalized spins interacting exclusively through their intrinsic dipolar interaction, as depicted in Fig. 1a. This interaction mediates the long-range hopping of spin-flip excitations. The quenching of the spin-flip band-structure owes to the anisotropy of the dipole-dipole interaction, which yields interference between different hopping directions [19]. The production of a synthetic background gauge potential is accomplished via spatially varying electromagnetic radiation [19, 20]. Together, the dipolar anisotropy and this radiation induce orientation-dependent Aharonov-Bohm phases that ultimately generate topologically nontrivial flat bands [19].

To be specific, we focus on an implementation using ultra-cold polar molecules trapped in a deep two-dimensional optical lattice. Such an implementation has many advantages, including local spatial addressing, stable long-lived spins, and strong intrinsic dipolar interactions [23–25, 27]. The molecules are subject to a static electric field $\vec{E}$ tilted with respect to the lattice plane (inset Fig. 1a). We assume that the molecular motion is pinned, and hence, restrict our attention to an effective rotational degree of freedom on each site, with associated Hamiltonian, $H_m = BJ^2 - d^z E$, where E is an applied electric field [26]. In particular, we focus on the four lowest rotational levels: $|0, 0\rangle$, the rovibrational ground state and the three states within the $J = 1$ manifold ($|1, -1\rangle$, $|1, 0\rangle$, $|1, 1\rangle$), where J characterizes the rotational angular momentum of the molecules. Here, the quantization axis, $\hat{z}$, lies along the applied electric field and $|J, m\rangle$ denotes the state adiabatically connected (via
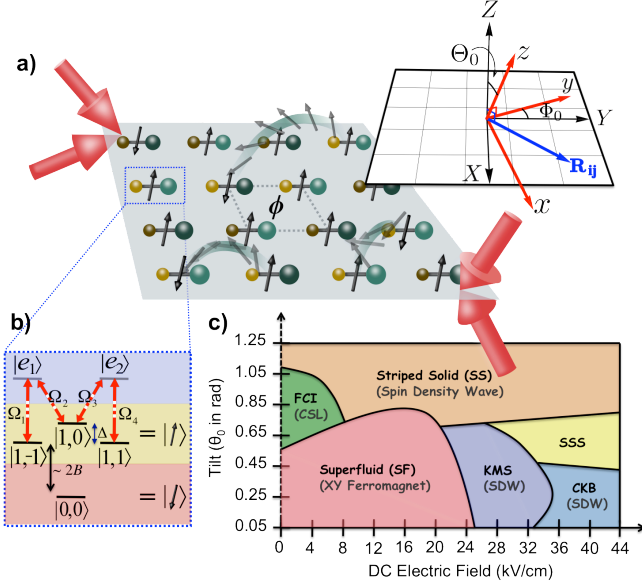
FIG. 1. Realization of a fractional Chern insulator. (a) Schematic representation of the two-dimensional array of polar molecules dressed by optical beams (red arrows). Each polar molecules is characterized as an effective pseudo-spin-flip, which can hop and interact mediated by the long-range dipolar interaction; ϕ represents the Aharanov-Bohm phase which the spin-flip acquires as it traverses a plaquette. (inset) Molecules occupy the $\{X, Y\}$ plane and the rotational quantization axis is set by an applied electric field along the $\hat{z}$ direction. Θ_0 and Φ_0 define the $\{x, y, z\}$ axes with respect to the lattice coordinates $\{X, Y, Z\}$. (b) We consider the $J = 0, 1$ manifolds of each molecule with the $|0, 0\rangle$ state representing spin-down. The spin-up state is created via optical Raman dressing in the M-configuration. The optical radiation admits a single dark eigenstate, which is a linear combination of the three states in the $J = 1$ manifold. (c) Phase diagram for $^{40}\mathrm{K}^{87}\mathrm{Rb}$ molecules at half-filling with a total of $N_s = 24$ sites as a function of electric field strength and tilt Θ_0. Each phase finds a direct analogy in the language of frustrated magnetism and the equivalent nomenclature is given below. The knight's move solid (KMS), checkerboard (CKB) and striped supersolid (SSS) are named for the position of bosons in the structure factor. The dotted line at $|E| = 0$ signifies the fact that a minimal electric field is always required to split the degeneracy within the $J = 1$ manifold.

$\vec{E}$) to the rotational eigenstates [28, 44]. Each molecule is driven by optical radiation, which couples the three $J = 1$ states to a pair of molecular excited states $|e_1\rangle$ and $|e_2\rangle$, in the so-called M-scheme (Fig. 1b). The Hamiltonian for each molecule with the laser on has the form $H_r = \hbar[\, |e_1\rangle(\Omega_1\langle 1, -1| + \Omega_2\langle 1, 0|) + |e_2\rangle(\Omega_3\langle 1, 0| + \Omega_4\langle 1, 1|) + \text{h.c.}\,]$ in the rotating frame, where Ω_i are Rabi frequencies serving as the control parameters. The above Hamiltonian admits a unique "dark" eigenstate, $|\uparrow\rangle = \frac{1}{\tilde{\Omega}}(\Omega_2\Omega_4|1, -1\rangle - \Omega_1\Omega_4|1, 0\rangle + \Omega_1\Omega_3|1, 1\rangle)$, which is decoupled both from the excited states and from the radiation field ($\tilde{\Omega}$ is a normalization). Together with the

rovibrational ground state, which we label as $|\downarrow\rangle$, this forms an effective two-state spin degree of freedom on each site [19, 28–32].

Individual molecules interact with one another via electric dipole-dipole interactions,

$$H_{dd} = \frac{1}{2}\sum_{i \neq j}\frac{\kappa}{R_{ij}^3}\left[\mathbf{d}_i \cdot \mathbf{d}_j - 3(\mathbf{d}_i \cdot \hat{\mathbf{R}}_{ij})(\mathbf{d}_j \cdot \hat{\mathbf{R}}_{ij})\right], \quad (1)$$

where $\kappa = 1/(4\pi\epsilon_0)$ and $\mathbf{R}_{ij}$ connects molecules i and j. The dipole moment operator ($\mathbf{d}_i$ and $\mathbf{d}_j$) of each polar molecule couples its internal rotational levels and is directed along the internuclear axis. We let d be the permanent molecular dipole moment and R_0 be the nearest-neighbor lattice spacing; we note that d, although related, is not the effective dipole moment of our pseudospins [44]. By ensuring that the characteristic dipolar interaction strength, $\kappa d^2/R_0^3$, is much weaker than the optical dressing, Ω_i, all molecules remain within the Hilbert space spanned by $\{|\uparrow\rangle, |\downarrow\rangle\}$. Moreover, this interaction is also much weaker than the bare rotational splitting $2B$ (Fig. 1b) and thus cannot cause transitions that change the total number of $|\uparrow\rangle$ excitations. This effective conservation law suggests the utility of recasting the system in terms of hardcore bosonic operators, $a_i^\dagger = |\uparrow\rangle\langle\downarrow|_i$, which create spin-flip "particles". Mediated by the dipolar interaction, these molecular spin-flips hop from site j to site i with amplitude $t_{ij} = -\langle\uparrow_i\downarrow_j|H_{dd}|\downarrow_i\uparrow_j\rangle$. As each hardcore boson harbors an electric-field induced dipole moment, there also exist long-range density-density interactions of strength $V_{ij} = \langle\uparrow_i\uparrow_j|H_{dd}|\uparrow_i\uparrow_j\rangle + \langle\downarrow_i\downarrow_j|H_{dd}|\downarrow_i\downarrow_j\rangle - \langle\uparrow_i\downarrow_j|H_{dd}|\uparrow_i\downarrow_j\rangle - \langle\downarrow_i\uparrow_j|H_{dd}|\downarrow_i\uparrow_j\rangle$. In combination, this yields a two-dimensional model of hardcore lattice bosons [44],

$$H_B = -\sum_{ij} t_{ij} a_i^\dagger a_j + \frac{1}{2}\sum_{i \neq j} V_{ij} n_i n_j, \quad (2)$$

whose total number, $N = \sum_i a_i^\dagger a_i$, is conserved [19, 44]. Variations in the dipolar-induced on-site potential, t_{ii}, can be regulated via tensor shifts from the optical lattice [44].

To ensure that our effective hardcore bosons reside in a topological flat band, we adjust the optical beams that dress the molecules to produce a square lattice with four types of sites, $\{a, b, A, B\}$, as shown in Fig. 2a [44]. Owing to interference between the dressing lasers, the dark state on each of the sites is a *different* linear combination of the three $J = 1$ states, implying that the hardcore boson, $a_i^\dagger$, is site-dependent. Despite the existence of four unique lattice sites, so long as t_{ij} and V_{ij} remain invariant under translations by the direct lattice vectors $\vec{g_1}$ and $\vec{g_2}$ (Fig. 2a), the Hamiltonian retains a two-site unit cell. Thus, computing the single-particle band-structure produces two bands in momentum space, with the bottom band possessing nonzero Chern number, $C = -1$, as shown in Fig. 2b [19].
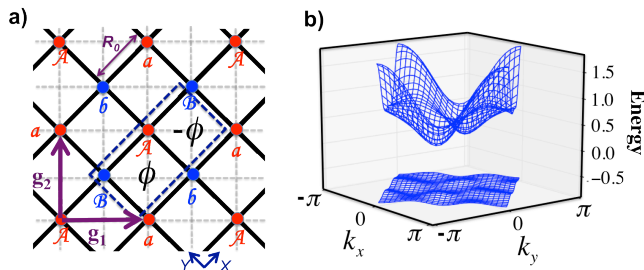
FIG. 2. Topological Flat Bands. (a) Schematic representation of the 2D dipolar array. a, b, A and B sites are characterized by dark eigenstates that are different linear combinations of the three $J = 1$ states. Square plaquettes are characterized by a time-reversal breaking flux, ϕ, which is staggered throughout the lattice. The lattice harbors a two-site unit cell and is invariant under translation by direct lattice vectors $\vec{g}_1$ and $\vec{g}_2$. (b) An optimized band-structure in the reduced Brillouin zone (RBZ) depicting a flatness ratio $f \approx 11.5$. The lowest band carries Chern index $C = -1$. The electric field tilt is $\{\Theta_0, \Phi_0\} = \{0.68, 5.83\}$ and the electromagnetic driving parameters are detailed in the supplemental information.

TABLE I. Diagnostics of Many-body Phases

Phase	Degeneracy	SF Response	Structure Factor	σ_{xy}
FCI	2	none	fluid	-0.5
SF	1	isotropic	fluid	gapless
SSS	3	uni-directional	stripes	gapless
KMS	4	none	knight's move	0
CKB	2	none	checkerboard	0
SS	4	none	stripes	0

Numerical optimization of the electric-field and the optical dressing yields a variety of flat bands. The optimized band-structure depicted in Fig. 2b has a flatness ratio [16–18], $f \approx 11.5$, and is obtained at weak DC electric fields, just strong enough to split the degeneracy within the $J = 1$ manifold (relative to the dipolar interaction strength) and to set the quantization axis [24].

With topological flat bands in hand, we now consider the actual many-body phases which arise at finite lattice filling fractions ν (number of spin flips per unit cell). To this end, we perform exact diagonalization of the full many-body Hamiltonian at $\nu = 1/2$ on systems of varying sizes up to $N_s = 44$ sites with periodic boundary conditions. For weak electric fields tilted near the so-called magic angle, $\Theta_0 = \cos^{-1}(1/\sqrt{3})$ [33], diagonalization reveals the existence of a bosonic $\nu = 1/2$ fractional Chern insulator. As numerical diagnostics, this topological state requires the presence of two-fold ground-state degeneracy on a torus (Fig. 3a) and a neutral spectral gap that is stable as the system size increases (Fig. 3b). The quantity analogous to the Hall conductance, $\sigma_{xy} = \frac{1}{2\pi} \int \int F(\theta_x, \theta_y) d\theta_x d\theta_y = -0.5$, appears unambiguously in the response of the system to boundary-condition twists $\{\theta_x, \theta_y\}$ (equivalent to flux insertion) in the form of a well-quantized many-body Berry curvature, $F(\theta_x, \theta_y) = \text{Im}(\langle \frac{\partial \Psi}{\partial \theta_y} | \frac{\partial \Psi}{\partial \theta_x} \rangle - \langle \frac{\partial \Psi}{\partial \theta_x} | \frac{\partial \Psi}{\partial \theta_y} \rangle)$ [2, 5, 7].

The counting statistics of low energy quasihole states provide a direct diagnostic of the fractionalization of removed particles [2, 35]. Counting the total number of admissible quasihole arrangements on a torus (for a $\nu = 1/2$ FCI) yields, $Q_{torus} = \binom{N_{uc}+1-N_b}{N_{uc}+1-2N_b} - \binom{N_{uc}-1-N_b}{N_{uc}+1-2N_b}$, where $N_{uc} = N_s/2$ is the number of lattice unit cells and N_b is the number of hardcore bosons. As depicted in Fig. 3c

for our system, numerically counting the total number of quasihole states matches the above formula precisely.

Remaining at $\nu = 1/2$, we now probe the many-body phases which arise as one varies the DC field strength and the tilt, Θ_0, while adjusting the optical parameters to keep the local dark states fixed [44]. Changes in the tilt alter the geometry of the dipoles and introduce additional dispersion into the single-particle bands. On the other hand, increasing the electric field strength enhances the long-range interactions. These qualitative differences in the microscopics yield a rich phase diagram exhibiting both conventional and topological phases, as shown in Fig. 1c. In addition to the FCI phase, there exist four distinct crystalline phases at strong DC fields and a large superfluid region at moderate fields (see Table I for diagnostics and [44] for details). While we use the language of lattice bosons above, we note that the FCI phase may also be interpreted in the language of frustrated magnetism as a chiral spin liquid while the competing superfluid and crystalline phases correspond to XY ordered magnetic and spin density wave (SDW) phases [13, 34].

Preparation and Detection—Next, we consider a possible route to preparing the $\nu = 1/2$ fractional Chern insulator. In current polar molecule experiments, the spin-flip "vacuum", corresponding to all sites in the $|\downarrow\rangle$ state, may be prepared with high fidelity from Feshbach molecules by two-photon stimulated Raman adiabatic passage [24, 36, 37]. If the phase boundaries surrounding the FCI state are second order, one might attempt to prepare this state by adiabatically tuning the electric field across the transition. However, the only known continuous transition between a superfluid and the $\nu = 1/2$ FCI phase is multicritical [38], which suggests that this phase boundary is generically first order, consistent with the numerics presented in the inset of Fig. 3d. On the other hand, continuous Mott insulator to FCI transitions are less finely tuned and may constitute a promising avenue for preparation. In particular, the striped solid phase may be reduced to a simple non-translation-symmetry breaking Mott insulator in the presence of a one-dimensional superlattice potential. This observation is consistent with the existence of a weaker, finite-size, cross-over at the FCI to striped-solid phase boundary (inset Fig. 3d).

As probe light couples directly to the rotational motion of the dipoles, it is possible to measure the single spin-flip
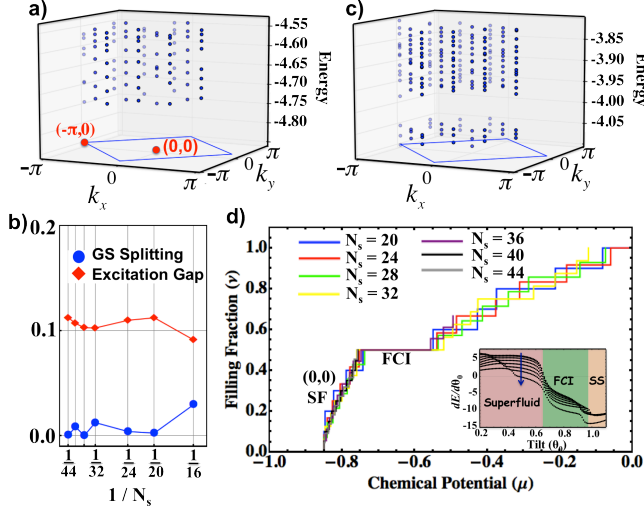
FIG. 3. Evidence for $\nu = 1/2$ FCI state. (a) Exact diagonalization of the full Hamiltonian at $\nu = 1/2$ with a total of $N_s = 24$ sites and $N_b = 6$ hardcore bosons. The electric field and driving parameters are identical to those used in Fig. 2b. To avoid self-interaction, we truncate the dipolar terms at order $1/(3R_0)^3$. There exist two degenerate ground states in momentum sectors $(k_x, k_y) = (0, 0)$ and $(k_x, k_y) = (-\pi, 0)$ consistent with a $\nu = 1/2$ FCI state on a torus (k_x, k_y are crystal momenta). (b) Finite size scaling from $N_s = 16$ to $N_s = 44$ suggests a stable spectral gap in the thermodynamic limit. (c) Quasihole counting for the same parameters as in (a) with a single boson removed ($N_b = 5$). There exists a clear gap below which there are 36 low-energy quasihole states, consistent with the analytical counting formula for Q_{torus} [2]. (d) Filling fraction as a function of chemical potential, $\mu = E_{N_b+1} - E_{N_b}$ (where E_{N_b} is the ground state energy with N_b bosons). Below $\nu = 1/2$, there exists evidence of a clear compressible superfluid state, while at $\nu = 1/2$, there exists a plateau indicative of an incompressible quantum liquid. This plateau can also be interpreted as a magnetization plateau in the language of frustrated magnetism [13, 14]. (inset) Depicts $dE/d\Theta_0$ as a function of tilt Θ_0. Phase transitions between the superfluid, Chern insulator and striped solid are evidenced as jumps in $dE/d\Theta_0$; the plateaus are rounded owing to finite size effects and the kink in the superfluid region arises from a jump between a zero-momentum and finite-momentum SF ground state. Curves from top to bottom are for increasing electric field strength from $E = 0.4 - 8$ kV/cm.

response of the system in order to detect and then characterize the FCI state. For example, the spectral function can be measured at finite energy and momentum using two-photon Bragg spectroscopy, providing direct infor-

mation regarding fractionalization [45–47]. On the edge, one should observe gapless chiral Luttinger liquid behavior, while in the bulk, the response should exhibit a gap to the multi-quasiparticle continuum. Such a gap manifests as an effective "magnetization" plateau as shown in Fig. 3d [13].

Experimental Realization— Our proposal can be carried out in currently available ultracold polar molecules, such as ^{40}K^{87}Rb [23], ^{7}Li^{133}Cs [37], ^{41}K^{87}Rb [36] and ^{87}Rb^{133}Cs [40–42]. The temperature scales associated with the FCI gap are set by the dipolar interaction strength. For a typical polar molecule with $d \sim 3$ Debye, the interaction at 532nm (optical lattice spacing) corresponds to $\sim 1\mu$K. With ground state molecules of both KRb and RbCs at temperatures of ~ 100nK, this suggests that current generation experiments can indeed realize stable FCI phases [24, 39, 41, 42, 44]. Moreover, it may be possible to work at significantly smaller optical lattice spacings (340nm for KRb and 395nm for RbCs), further enhancing the dipolar temperature scales [43].

Here, we focus on ^{40}K^{87}Rb. For the optically excited states $|e_1\rangle$ and $|e_2\rangle$, we propose the $|J', m'\rangle = |2, \pm 2\rangle$ rotational states of the $v' = 41$ vibrational level of the $(3)^1\Sigma^+$ electronic state. These states harbor a strong 640 nm transition to the ground state [24, 36]. We require a hierarchy of energy scales corresponding to, $H_{lattice} \lesssim H_{hf} \ll \Omega_i \ll \Delta$ (Fig. 1b), where $H_{lattice}$ describes the optical lattice potential and H_{hf} characterizes the molecule's hyperfine structure [24]. For ^{40}K^{87}Rb, this hierarchy is easily realized since $H_{hf} \sim 1$ MHz, while $\Delta = 160$ MHz at a moderate DC field strength, $E = B/d \approx 0.5$kV/cm. By ensuring that the optical dressing (Ω_i) is weak relative to the splitting, $E_{1,0} - E_{1,1}$, we can employ frequency selection during the creation of the M-scheme [44]; meanwhile, the condition $H_{lattice} \lesssim H_{hf} \ll \Omega_i$ allows us to consider hyperfine and tensor light-shift effects only after the dark state ($|\uparrow\rangle$) is already defined [44].

While we have focused our discussion on polar molecules, our proposal can, in fact, be realized in any system composed of electric or magnetic dipolar interacting generalized spins; such degrees of freedom are found in a diverse array of contexts ranging from magnetic atoms and Rydberg ensembles to solid-state spins [22, 48, 49]. In particular, for exchange coupled electronic spin dimers or hyperfine coupled nuclear and electronic spins, one finds an effective level-structure nearly identical to that depicted in Fig. 1b. The dipolar interaction between such coupled spins also yields topologically non-trivial, flat, spin-flip band-structures, enabling the potential realization of a solid-state Chern insulator [50].

[1] R. Roy and S. L. Sondhi. *Physics* **4**, 46 (2011).

[2] N. Regnault and B. Andrei Bernevig. *Phys. Rev. X* **1**, 021014 (2011).

[3] G. Moller and N. R. Cooper. *Phys. Rev. Lett.* **108**, 045306 (2012).

[4] S. A. Parameswaran, R. Roy, S. L. Sondhi. *Phys. Rev. B* **85**, 241308(R) (2012).

[5] D. N. Sheng, Z.-C. Gu, K. Sun, L. Sheng. *Nat. Commun.*

2, 389 (2011).

[6] Z. Liu, E. J. Bergholtz, H. Fan, A. M. Läuchli. *Phys. Rev. Lett.* **109**, 186805 (2012).

[7] Y.-F. Wang *et al. Phys. Rev. Lett.* **107**, 146803 (2011).

[8] J. McGreevy, B. Swingle and K.-A. Tran, *Phys. Rev. B* **85**, 125105 (2012).

[9] X.-G. Wen, *Phys. Rev. B* **65**, 165113 (2002).

[10] D. C. Tsui, H. L. Stormer, A. C. Gossard. *Phys. Rev. Lett.* **48**, 1559 (1982).

[11] R. B. Laughlin *Phys. Rev. Lett.* **50**, 1395 (1983).

[12] A. M. Essin, M. Hermele, arXiv:1212.0593 (2012).

[13] V. Kalmeyer and R. B. Laughlin *Phys. Rev. Lett.* **59**, 2095 (1987).

[14] V. Kalmeyer and R. B. Laughlin *Phys. Rev. B* **39**, 11879 (1989).

[15] A. E. B. Nielsen, J. I. Cirac, G. Sierra. *Phys. Rev. Lett.* **108**, 257206 (2012).

[16] K. Sun, Z. Gu, H. Katsura, and S. Das Sarma. *Phys. Rev. Lett.* **106**, 236803 (2011).

[17] E. Tang, J-W. Mei, and X-G. Wen. *Phys. Rev. Lett.* **106**, 236802 (2011).

[18] T. Neupert, L. Santos, C. Chamon, and C. Mudry. *Phys. Rev. Lett.* **106**, 236804 (2011).

[19] N. Y. Yao *et al Phys. Rev. Lett.* **109**, 266804 (2012).

[20] I. B. Spielman *Physics* **4**, 35 (2011).

[21] T. Giamarchi, Ch. Ruegg, O. Tchernyshyov, *Nature Phys.* **4**, 198 (2008).

[22] L. Childress *et al*, Science **314**, 281 (2006).

[23] K. K. Ni, S. Ospelkaus, M. H. G. de Miranda, A. Peer, B. Neyenhuis, J. J. Zirbel, S. Kotochigova, P. S. Julienne, D. S. Jin, and J. Ye, Science 322, 231 (2008).

[24] A. Chotia *et al. Phys. Rev. Lett.* **108**, 080405 (2012).

[25] D. Wang, B. Neyenhuis, M. H. G. de Miranda, K. K. Ni, S. Ospelkaus, D. S. Jin, and J. Ye, Phys. Rev. A 81, 061404(R) (2010).

[26] Brown, J. M. & Carrington, A. Rotational Spectroscopy of Diatomic Molecules. *Cambridge University Press* (2003).

[27] S. Ospelkaus *et al. Phys. Rev. Lett.* **104**, 030402 (2010).

[28] A. V. Gorshkov *et al. Phys. Rev. Lett.* **107**, 115301 (2011)

[29] A. Micheli, G. K. Brennen, & P. Zoller. *Nature Phys.* **2**, 341 (2006)

[30] A. Micheli, G. Pupillo, H. P. Buchler, and P. Zoller, *Phys. Rev. A* **76**, 043604 (2007).

[31] J. Aldegunde, B. A. Rivington, P. S. Zuchowski, and J. M. Hutson, *Phys. Rev. A* **78**, 033434 (2008).

[32] S. R. Manmana, E. M. Stoudenmire, K. R. A. Hazzard, A. M. Rey, A. V. Gorshkov, arXiv:1210.5518 (2012).

[33] E. R. Andrew, A. Bradbury, and R. G. Eades, *Nature* **182**, 1659 (1958).

[34] M. Greiter and R. Thomale, *Phys. Rev. Lett.* **102**, 207203 (2009).

[35] B. A. Bernevig and N. Regnault , *Phys. Rev. B* **85**, 075128 (2012).

[36] K. Aikawa *et al. Phys. Rev. Lett.* **105**, 203001 (2010).

[37] J. Deiglmayr *et al. Phys. Rev. Lett.* **101**, 133004 (2008).

[38] M. Barkeshli, J. McGreevy. arXiv:1201.4393v1 (2012).

[39] C.-H. Wu, J. W. Park, P. Ahmadi, S. Will, and M. W. Zwierlein, Phys. Rev. Lett. 109, 085301 (2012).

[40] A. J. Kerman *et al*, Phys. Rev. Lett. 92, 033004 (2004).

[41] T. Takekoshi *et al*, Phys. Rev. A 85, 032506 (2012).

[42] *private communication* F. Schreck

[43] S. Kotochigova and E. Tiesinga, Phys. Rev. A 73, 041405(R) (2006).

[44] See Supplemental Material at http://link.aps.org/ supplemental/ for methods and theoretical derivations.

[45] N. Goldman, J. Beugnon, F. Gerbier. *Phys. Rev. Lett.* **108**, 255303 (2012).

[46] J. A. Kjall, J. E. Moore. arXiv:1112.1800v1 (2012).

[47] H. Guo, C.-C. Chien, and K. Levin. *Phys. Rev. Lett.* **105**, 120401 (2010).

[48] J. D. Pritchard *et al. Phys. Rev. Lett.* **105**, 193603 (2010).

[49] M. Lu, S.-H. Youn, B. Lev, *Phys. Rev. Lett.* **104**, 063001 (2010).

[50] N. Y. Yao *in preparation.*